ARTICLES
https://doi.org/10.1038/s41563-018-0250-y
nature materials

Dislocation-induced thermal transport anisotropy in single-crystal group-III nitride films

Bo Sun[1,5], Georg Haunschild[2], Carlos Polanco[3], James (Zi-Jian) Ju[2], Lucas Lindsay[3], Gregor Koblmüller[2] and Yee Kan Koh[1,4*]

Dislocations, one-dimensional lattice imperfections, are common to technologically important materials such as III–V semiconductors, and adversely affect heat dissipation in, for example, nitride-based high-power electronic devices. For decades, conventional nonlinear elasticity models have predicted that this thermal resistance is only appreciable when the heat flux is perpendicular to the dislocations. However, this dislocation-induced anisotropic thermal transport has yet to be seen experimentally. Using time-domain thermoreflectance, we measure strong thermal transport anisotropy governed by highly oriented threading dislocation arrays throughout micrometre-thick, single-crystal indium nitride films. We find that the cross-plane thermal conductivity is almost tenfold higher than the in-plane thermal conductivity at 80 K when the dislocation density is ~3×10^{10} cm^{-2}. This large anisotropy is not predicted by conventional models. With enhanced understanding of dislocation–phonon interactions, our results may allow the tailoring of anisotropic thermal transport with line defects, and could facilitate methods for directed heat dissipation in the thermal management of diverse device applications.

Over the past decade, accurate experiments[1,2] and theoretical methods[3–7] have significantly advanced the knowledge about lattice imperfections (point defects, dislocations, grain boundaries and so on) and how these impede thermal transport in crystals and nanostructures. This in-depth understanding has facilitated better thermal management of electronic and optoelectronic devices[8] and the design of thermoelectric materials[9]. Unlike other defects, the role of dislocations in thermal resistance remains poorly understood. From a theoretical perspective, predictive first-principles calculations[3–5] of phonon scattering by dislocations is still nascent, partly due to the large supercells required for their description. Thus, most recent theoretical efforts have relied on conventional nonlinear elasticity models[10–13], as pioneered by Klemens in the mid-1950s, to describe dislocation–phonon interactions.

According to these conventional theories, phonons are elastically scattered by dislocations by two distinct mechanisms: static scattering[10–12] and dynamic scattering[13,14]. Dynamic scattering occurs when mobile dislocations resonantly absorb an incident phonon, vibrate and re-emit a phonon through the process. To have resonant phonon–dislocation interactions, the phonon wavelengths must be comparable to the distance between two pinning points in the dislocations[15]. Phonons with such characteristically long wavelengths are important for heat conduction only at low temperatures (for example, <10 K), and thus dynamic scattering is insignificant for heat transport at elevated temperatures[13]. Static scattering, on the other hand, can arise from the cores of the dislocations as well as from the strain field generated by these dislocations. At short range, phonons are scattered by the distortion of the lattice in the immediate vicinity of the cores. At long range, phonons are scattered by the anharmonicity related to the inhomogeneous strain fields induced by the dislocations. Klemens first treated this static scattering using perturbation theory, and found that scattering by the long-range strain fields is much stronger than scattering by the cores at temperatures lower than the Debye temperature[10]. Carruthers used a more rigorous strain field displacement in the scattering matrix, and derived a scattering cross-section ~1,000 times larger than the expression by Klemens for edge-type dislocations[11]. Neither of these conventional models, however, universally and quantitatively describes the experimental data currently available[13,14].

One distinct prediction of nonlinear elasticity models is that only phonons that propagate perpendicular to the dislocations are strongly scattered, due to the planar strain field generated by both edge-type and screw-type dislocations[10,12]. This phonon scattering anisotropy could give rise to large anisotropy in thermal conductivity if dislocations are highly oriented. While large anisotropy in thermal conductivity has been observed in crystals with layered structures (for example, graphite[16], transition metal dichalcogenides[17] and black phosphorus[18]), this behaviour originates mainly from the anisotropic crystal structures (for example, anisotropy in phonon velocity[17,18]) and not from anisotropy in scattering by extrinsic defects. The predicted anisotropy in thermal transport due to dislocation–phonon interactions has not been verified by experiment due to the challenges of synthesizing single-crystal materials with a large density of highly oriented dislocations and of accurately measuring their thermal conductivity, both cross-plane and in-plane. Previous measurements taken to study phonon–dislocation interactions were performed on bulk samples with a low density of uncontrolled, random dislocations, and only isotropically reduced thermal conductivities were reported[13,15,19,20,21].

In this Article we experimentally demonstrate strongly anisotropic thermal transport in single-crystalline semiconductors with highly oriented dislocation arrays. In particular, we exploit here the unique properties of wurtzite, that is, (0001)-oriented group-III nitrides, which form vertically well-oriented threading dislocations along the growth direction upon heteroepitaxy on lattice-mismatched substrates, exemplified here for the case of InN

[1]Department of Mechanical Engineering, National University of Singapore, Singapore, Singapore. [2]Walter Schottky Institute, Department of Physics, Technical University of Munich, Garching, Germany. [3]Materials Science and Technology Division, Oak Ridge National Laboratory, Oak Ridge, TN, USA. [4]Centre of Advanced 2D Materials, National University of Singapore, Singapore, Singapore. [5]Present address: Tsinghua-Berkeley Shenzhen Institute, Tsinghua University, Shenzhen, China. *e-mail: mpekyk@nus.edu.sg

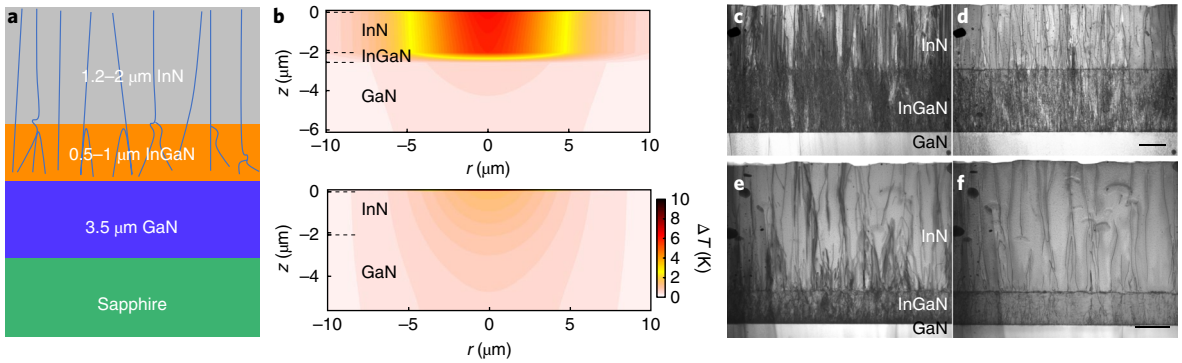

Fig. 1 | InN structure design and characterization. a, Schematic diagram of our InN samples with oriented threading dislocations (not to scale). **b**, Amplitudes of temperature oscillations of Al (100 nm) on a 2 μm InN film on a GaN substrate, with (top) and without (bottom) a 0.5 μm InGaN layer, with periodic heating at a frequency of 0.5 MHz and a Gaussian distribution heating intensity ($1/e^2$ radius = 5 μm), calculated using thermal properties at 80 K. $r = 0$ locates the centre of the Gaussian profile while $z = 0$ is the sample surface. **c–f**, Cross-sectional TEM images of the InN films with threading dislocation densities of 2.9×10^{10} cm^{-2} (**c**,**d**) and 1.1×10^{10} cm^{-2} (**e**,**f**). Edge-type (**c**,**e**) and screw-type (**d**,**f**) threading dislocations are imaged at diffraction vectors $g = 1\bar{1}00$ and $g = 0002$, respectively. Scale bars, 500 nm.

on GaN. Our results provide the first unambiguous evidence for dislocation-induced anisotropic thermal transport, and thus confirm this prediction by Klemens from six decades ago[10]. Furthermore, comparison of the thermal conductivity of as-measured InN with that obtained from intrinsic ab initio calculations coupled with empirical models for phonon–dislocation interactions demonstrates that scattering strengths according to Carruthers' model are crudely comparable to the scattering strengths observed in our measurements, far better than the predictions of Klemens' model. However, neither model captures the temperature dependence of our measurements accurately. We provide possible explanations for the stronger-than-expected scattering observed at lower temperatures.

Anisotropic heat transport induced by oriented dislocations

We synthesized ~1.2- to 2-μm-thick heteroepitaxial wurtzite InN films on *c*-plane, (0001)-oriented GaN/sapphire substrates with an $In_{0.8}Ga_{0.2}N$ buffer layer (Fig. 1a) using plasma-assisted molecular beam epitaxy (PAMBE)[22,23]. We determined the density of threading dislocations in our InN films from X-ray rocking curves (ω scans) and cross-sectional transmission electron microcopy (TEM) under the two-beam condition (Fig. 1c–f and Supplementary Note 1). With TEM images taken at different diffraction conditions, edge-type (Fig. 1c–e) and screw-type (Fig. 1d–f) dislocations can also be selectively imaged and counted[22]. The density of pure edge- and mixed-type dislocations was found to be more than 20 times larger than that of pure screw-type dislocations, in agreement with recent studies of heteroepitaxial InN films grown on GaN/sapphire substrates[22,24]. This suggests that the prominent role of dislocation–phonon interactions and effects on thermal conductivity seen in our materials is due to edge- and mixed-type dislocations.

We measured the in-plane thermal conductivity $\Lambda_\parallel$ (perpendicular to dislocations) and the cross-plane thermal conductivity $\Lambda_\perp$ (along the dislocations) of the InN films using time-domain thermoreflectance (TDTR)[25,26]. Details of the implementation, analysis and uncertainty estimation of TDTR measurements are provided in the Methods and Supplementary Notes 2.1–2.5. For materials with highly anisotropic thermal properties, heat flows more readily in the direction of lower thermal resistance, that is, along the dislocations in our InN films (Fig. 1b). As a result, TDTR measurements of InN films alone are not sensitive to $\Lambda_\parallel$, which is pivotal for understanding the reduction in thermal conductivity by dislocations. To overcome this challenge, we inserted an InGaN buffer layer (with low thermal conductivity) beneath the InN film, to direct heat flow to the in-plane direction (Fig. 1b), and thus substantially improved the sensitivity of our $\Lambda_\parallel$ measurements. To ensure the accuracy of the measurements, we also employed two newly developed approaches, beam-offset TDTR[27] and dual-frequency TDTR[28], on a few selected data points. In beam-offset TDTR, heating by the pump beam and measurements by the probe beam are offset laterally, such that measurements are only sensitive to $\Lambda_\parallel$ and not $\Lambda_\perp$. Dual-frequency TDTR, on the other hand, is a differential method, in which an additional measurement is performed at a low modulation frequency to reduce the sensitivity to the sources of uncertainties for $\Lambda_\perp$ measurements. Thermal conductivities determined from these methods agree within measured uncertainty (Supplementary Note 2.6). We also note that our approach includes a correction that accounts for artefacts due to leaked pump beam arising from the surface roughness of the samples[26].

Figure 2a and Supplementary Fig. 12 in Supplementary Note 3 present the measured in-plane ($\Lambda_\parallel$) and cross-plane ($\Lambda_\perp$) thermal conductivities of our InN films as a function of temperature T. In contrast to the small anisotropy induced by other extrinsic defects (for example, boundary scattering[29,30]), we observe a large dislocation-induced anisotropy in the low-T thermal conductivity of our InN films with oriented threading dislocations, which is very sensitive to T (Fig. 2b). The intrinsic anisotropy of InN due to its wurtzite structure is small and independent of T, with an anisotropy ratio[4] of only <1.17 (see our first-principles calculations in Fig. 2b). We contrast the anisotropic thermal conductivity of our InN films with previously reported, structurally induced anisotropic thermal conductivities of other materials in Fig. 2b[16–18,29–32]. The anisotropy we observe is fundamentally different in three important aspects. First, previous reports have demonstrated structurally induced anisotropies that are not easily manipulated, while here we demonstrate defect-induced thermal conductivity anisotropy, which can be engineered. Second, all previously reported measurements have suppressed thermal conductivity in the through-plane crystallographic orientation, while the measured thermal conductivity of our InN films is subdued along the basal plane (Fig. 2a,b; open versus filled symbols). In the cross-plane direction, $\Lambda_\perp$ of our InN films approaches the intrinsic thermal conductivity of InN predicted by our first-principles calculations, with a temperature dependence of roughly T^{-1}. Meanwhile, in the in-plane direction, $\Lambda_\parallel$ of our InN films is strongly suppressed at low T. Third, as a result of the unique T dependence of $\Lambda_\parallel$ in our InN films, the anisotropy ratios of our measurements exhibit a strong T dependence (Fig. 2b). This T dependence is starkly different

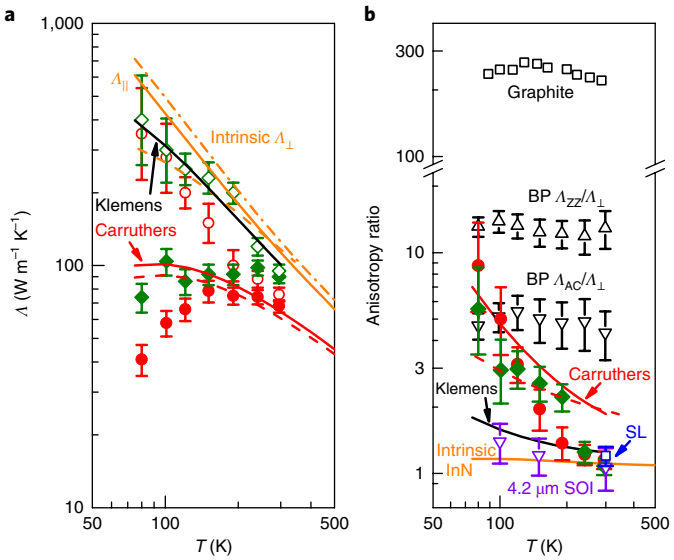

Fig. 2 | Temperature-dependent thermal conductivity of InN films with oriented threading dislocations. a, In-plane $\Lambda_{\parallel}$ (filled symbols) and cross-plane $\Lambda_{\perp}$ (open symbols) thermal conductivity of InN films with dislocation densities of 1.1×10^{10} cm^{-2} (green diamonds) and 2.9×10^{10} cm^{-2} (red circles). The intrinsic thermal conductivities $\Lambda_{\parallel}$ (solid orange curve) and $\Lambda_{\perp}$ (dash-dotted orange curve) of InN are calculated from first principles. The in-plane thermal conductivity including phonon–dislocation scattering from Carruthers' model[11] (red solid curve) and Klemens' model[10] (black solid curve), for a dislocation density of 2.9×10^{10} cm^{-2}, are included for comparison. To assess the effects of boundary scattering, first-principles calculations of $\Lambda_{\perp}$ (dashed orange curve) and $\Lambda_{\parallel}$ with dislocations from Carruthers' model (dashed red curve) with an additional boundary scattering term are also included. There are no adjustable parameters in the empirical calculations. Estimation of error bars is detailed in Supplementary Note 2.5. **b**, Temperature-dependent anisotropy ratios of InN films with a dislocation density of 1.1×10^{10} cm^{-2} (green diamonds) and 2.9×10^{10} cm^{-2} (red circles), compared to the anisotropy ratios of graphite (black squares[16]), black phosphorus (black triangles[18], the in-plane thermal conductivities in zigzag and armchair directions are labelled as Λ_{ZZ} and Λ_{AC}, respectively), GaAs/AlAs superlattice (blue square[29]) and 4.2-μm-thick silicon-on-insulator (SOI, purple triangles[31,32]). The filled symbols represent $\Lambda_{\perp}/\Lambda_{\parallel}$, while the open symbols represent $\Lambda_{\parallel}/\Lambda_{\perp}$. The anisotropy ratios of the intrinsic thermal conductivity of InN from our first-principles calculations (orange solid curve), and with a dislocation density of 2.9×10^{10} cm^{-2} calculated using Klemens' model (black solid curve) and Carruthers' model with (red dashed curve) and without (red solid curve) the additional boundary scattering are also presented. Error bars are the root of sums of squares of the uncertainties of $\Lambda_{\parallel}$ and $\Lambda_{\perp}$ in **a**.

from previously reported thermal conductivity anisotropies, which are largely T independent[16,18]. At room temperature, $\Lambda_{\parallel}$ and $\Lambda_{\perp}$ of all our InN films are similar within experimental uncertainty. However, at low T, we observe large anisotropy for all our InN films, the extreme case being $\Lambda_{\perp}/\Lambda_{\parallel}\approx9$ at 80 K for the InN film with a dislocation density of 2.9×10^{10} cm^{-2}.

Origins of thermal transport anisotropy

The differences between our work and previously reported measurements demonstrate that thermal conductivity anisotropies as observed by the present InN films have a different origin. Previously reported thermal conductivity anisotropies originate from anisotropies in the crystal structure[17,18]. Substantially larger thermal conductivities along the basal plane have been reported for crystals with highly anisotropic phonon dispersions (and thus anisotropic phonon velocity), such as black phosphorus[18] and graphite[16]. Moreover, anisotropic crystal structures could also result in anisotropic scattering of phonons. For example, we previously demonstrated that anisotropy in the thermal conductivity of black phosphorus in the basal planes is mainly due to anisotropy in phonon dispersion, while the low through-plane thermal conductivity partially originates from enhanced Umklapp scattering across the basal planes[18]. For these structure-induced anisotropies, phonons are predominantly scattered in all crystallographic directions by the same phonon–phonon scattering process with the same T dependence[4,18]. As a result, the anisotropy ratios of these crystals are largely T independent (Fig. 2b).

By contrast, the unique T-dependent anisotropy we observe in our measurements indicates that phonons are predominantly scattered by different mechanisms in the in-plane and cross-plane directions of the InN films. In the cross-plane direction, we observe that $\Lambda_{\perp}$ is roughly proportional to T^{-1}. This T dependence suggests that in the cross-plane direction phonons are predominantly scattered by three-phonon Umklapp processes[4,18]. On the other hand, in the in-plane direction, we attribute the strong suppression of $\Lambda_{\parallel}$ at low T to the anisotropic scattering by dislocations. The suppression of heat conduction only in the in-plane direction cannot be explained by other extrinsic scattering mechanisms, such as point defects, interfaces and grain boundaries, as these scattering mechanisms inevitably impede heat flow in both in-plane and cross-plane directions[31,32]. While boundary scattering can also result in thermal conductivity anisotropies[33] (see the anisotropy of GaAs/AlAs superlattices[29] and Si thin films[30–32] in Fig. 2b), the anisotropy is relatively small and thermal transport is more strongly suppressed in the cross-plane direction[29–32], opposite to that seen in our measurements of thermal conductivities in InN films with dislocations. To demonstrate the effects of boundary scattering to the thermal transport anisotropy, we include an additional boundary scattering term in the calculations of intrinsic $\Lambda_{\perp}$ and $\Lambda_{\parallel}$ of InN with dislocations (see the dashed curves in Fig. 2). The details of the calculations are provided in Supplementary Note 4. We find that boundary scattering more strongly reduces $\Lambda_{\perp}$ than $\Lambda_{\parallel}$ (Fig. 2a) and thus reduces the anisotropy ratio $\Lambda_{\perp}/\Lambda_{\parallel}$ (Fig. 2b). Hence, our results unambiguously demonstrate dislocation-induced thermal conductivity anisotropy as predicted by Klemens[10].

Empirical models for dislocation–phonon interactions

Our measurements of anisotropic thermal conductivity provide critical data with which to understand dislocation–phonon interactions. To further examine these interactions and their role in determining anisotropic thermal transport, we calculated the thermal conductivity of the InN films with oriented threading dislocations from a full solution of the Peierls–Boltzmann transport equation combining ab initio three-phonon and isotope scattering rates with different empirical models for phonon–dislocation scattering rates (see Methods for details). We only consider static scattering by dislocation cores and long-range strain fields using Klemens' and Carruthers' models[10,11], as dynamic scattering by dislocations is significant only at low T. Our calculations indicate that the commonly used Klemens model[10] underestimates the strength of phonon–dislocation scattering, resulting in thermal conductivity values over an order of magnitude larger than experimental data at low T (Fig. 2a). This deficiency, also found in LiF samples[19], motivated Carruthers to use a logarithmic strain field displacement, which increases the scattering strength[11]. Figure 2a shows the prediction of thermal conductivity when the Carruthers model is used. The order-of-magnitude similarity between calculated values and experimental data around room temperature is impressive given the many simplifications of the model and absence of fitting parameters. Nevertheless, Carruthers' model underpredicts the scattering strength by dislocations, especially at low T, and thus

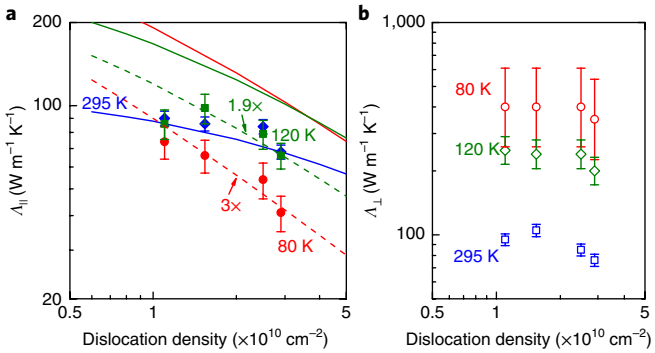

Fig. 3 | Dislocation density-dependent thermal transport. a,**b**, In-plane (**a**, filled symbols) and cross-plane (**b**, open symbols) thermal conductivity of InN films as a function of N_d at 80 K (red), 120 K (green) and 295 K (blue). Solid curves are the first-principles calculations with Carruthers' model for phonon–dislocation scattering at the respective temperatures, while dashed curves are calculations with the strength of phonon–dislocation interactions 3× and 1.9× of that predicted by Carruthers, as labelled. Error bars are calculated as in Fig. 2.

does not capture the T behaviour of thermal conductivity for different dislocation densities (Fig. 2a).

We consider a few possible reasons for the failure of Carruthers' model to capture the T dependence of the in-plane thermal conductivity of the InN films. One possible explanation for the stronger reduction in $\Lambda_{\parallel}$ at cryogenic temperatures is additional scattering by the boundaries of crystallites (or effectively multicrystalline environment due to the dense array of dislocations) in the in-plane direction. Our X-ray rocking curves and TEM images, however, provide evidence that our InN films are single crystals with the same crystallographic orientations, rather than polycrystalline material. X-ray rocking curves (Supplementary Fig. 2) show only peaks of (0002) of InN, demonstrating this. TEM images using the two-beam condition are also consistent with Bragg's law for single-crystal InN. Moreover, the average inter-dislocation spacings in our samples are larger than 60 nm, with dislocations randomly distributed in the in-plane direction. Since the strain field around a single dislocation is only few nanometers[34], the inter-dislocation spacings are too large for such effective multicrystalline environment.

Another possible explanation for the observed T dependence is omission of scattering by the dislocation cores in Carruthers' model. However, we find that scattering by dislocation cores is negligible[10], even at room temperature where these are predicted to be more important. (See the calculations with and without scattering by dislocation cores in Supplementary Fig. 14.)

Also, the weaker scattering at low T predicted by the empirical models could be due to neglecting the overlapping of dislocation strain fields, as the models only treat phonon scatterings from single dislocations, which is probably valid at low dislocation densities. The collective effects of overlapping strain fields at higher densities may scatter long-wavelength phonons preferentially. In our InN films, the dislocation densities are large, with an average inter-dislocation spacing of only 60–100 nm. At low T, the wavelength of phonons in InN that carry the majority of heat could be comparable to the inter-dislocation spacing, and thus the assumption of isolated dislocations is violated. To evaluate this possibility, we plot the accumulated thermal conductivity as a function of phonon wavelength in Supplementary Fig. 13. We find that the wavelengths of heat-carrying phonons are mostly <5 nm even at 80 K, not sufficiently large to be coupled with the periodic strain fields in our samples.

Finally, the empirical models might underestimate the scattering rate due to neglecting the change of interatomic forces in the vicinity of dislocation cores. A recent ab initio calculation of phonon scattering by the cores of dislocations, without considering long-range strain field effects, showed larger scattering rates than those predicted by analytical models for Si[5]. These larger scattering rates were attributed to changes in the interatomic force constants in the neighbourhood of the dislocation, which are not properly treated by first-order perturbation approaches[5–7,35] in Klemens' and Carruthers' models. Similar ab initio methods could provide insights here; however, these are beyond our current computational resources due to the large supercells required to model dislocations with long-range strain field.

Dependence on dislocation density

To obtain a clearer picture of the effect of threading dislocations on thermal transport, we plotted $\Lambda_{\parallel}$ and $\Lambda_{\perp}$ as a function of dislocation density (N_d) (Fig. 3) and compared the results with our first-principles calculations with the phonon–dislocation interactions approximated by Carruthers' model (solid lines) and when enhanced by up to 3× (labelled in the figure, dashed lines). At room temperature, $\Lambda_{\parallel}$ and $\Lambda_{\perp}$ are similar for all samples despite the variation in dislocation density, and the weak dependence on N_d agrees with the calculations using Carruthers' model. We note that the overall high dislocation density of our samples (~10^{10} cm^{-2}) is insufficient to diminish the intrinsic thermal conductivity of InN appreciably, indicating that phonon–dislocation scattering is comparable or weaker than the intrinsic phonon–phonon scattering with this dislocation density (see comparison of the scattering rates of different scattering mechanisms in Supplementary Fig. 14). For $\Lambda_{\perp}$, we do not observe any noticeable change with N_d even at 80 K, suggesting that phonons are not strongly scattered along the dislocation lines. For $\Lambda_{\parallel}$, however, we observe a fairly strong dependence on N_d at 80 K, consistent with our argument that the suppression of the in-plane thermal conductivity at lower temperatures is due to oriented dislocations. The dependence can be roughly approximated by Carruthers' model with a 3× enhanced scattering strength, further strengthening our previous claim that Carruthers' model underestimates the phonon–dislocation strength at cryogenic temperatures.

Finally, we used Carruthers' model to estimate the impact of dislocations on the thermal conductivity of GaN (Supplementary Fig. 16a in Supplementary Note 5). In the calculations, we also included phonon scattering from Ga vacancies (as mass variance only) with densities of 10^{18} cm^{-3} and 10^{20} cm^{-3}. We find that for GaN with a vacancy density of 10^{18} cm^{-3}, heat transfer in GaN is dominated by scattering by dislocations when the dislocation density is larger than 10^{9} cm^{-2}, which is not uncommon in GaN films and devices. We also calculated $\Lambda_{\parallel}$ (perpendicular to dislocations) and $\Lambda_{\perp}$ (along dislocations) of GaN and plotted $\Lambda_{\perp}/\Lambda_{\parallel}$ as a function of temperature for dislocation densities ranging from 10^{9} to 10^{12} cm^{-2} (Supplementary Fig. 16b). For dislocation densities of 10^{9} cm^{-2} and 10^{10} cm^{-2}, we find that anisotropy in thermal transport disappears at ~400 K and ~1,000 K, respectively.

Outlook

Our results add an important degree of freedom for the thermal management of nitride-based electronic and optoelectronic devices, and designs for directed heat dissipation for electronic devices[8]. III-nitride semiconductors, such as GaN, AlN, InN and their related compounds, are promising materials in a wide range of emerging applications, such as power electronics and light-emitting diodes (LEDs). Efficient thermal management of these devices requires a detailed understanding of phonon scattering by dislocations, commonly found in III-nitrides due to the limitations of current growth techniques[23]. Also, we present a route to anisotropically direct heat flow via dislocations, which could be used to guide and spread heat in electronic devices. Unlike previous anisotropic heat transport that relies on material crystal structures, the anisotropic heat

transport presented here originates from crystal defects, which may be manipulated and implanted independent of crystal geometry.

Online content

Any methods, additional references, Nature Research reporting summaries, source data, statements of data availability and associated accession codes are available at https://doi.org/10.1038/s41563-018-0250-y.

Received: 7 April 2018; Accepted: 14 November 2018;
Published online: 17 December 2018

References

1. Li, D. et al. Thermal conductivity of individual silicon nanowires. *Appl. Phys. Lett.* **83**, 2934–2936 (2003).
2. Chen, S. et al. Thermal conductivity of isotopically modified graphene. *Nat. Mater.* **11**, 203–207 (2012).
3. Broido, D. A., Malorny, M., Birner, G., Mingo, N. & Stewart, D. A. Intrinsic lattice thermal conductivity of semiconductors from first principles. *Appl. Phys. Lett.* **91**, 231922 (2007).
4. Ma, J., Li, W. & Luo, X. Intrinsic thermal conductivity and its anisotropy of wurtzite InN. *Appl. Phys. Lett.* **105**, 082103 (2014).
5. Wang, T., Carrete, J., van Roekeghem, A., Mingo, N. & Madsen, G. K. H. Ab initio phonon scattering by dislocations. *Phys. Rev. B* **95**, 245304 (2017).
6. Katre, A., Carrete, J., Dongre, B., Madsen, G. K. H. & Mingo, N. Exceptionally strong phonon scattering by B substitution in cubic SiC. *Phys. Rev. Lett.* **119**, 075902 (2017).
7. Polanco, C. A. & Lindsay, L. Ab initio phonon point defect scattering and thermal transport in graphene. *Phys. Rev. B* **97**, 014303 (2018).
8. Yan, Z., Liu, G., Khan, J. M. & Balandin, A. A. Graphene quilts for thermal management of high-power GaN transistors. *Nat. Commun.* **3**, 827 (2012).
9. Zhang, Q. et al. High thermoelectric performance by resonant dopant indium in nanostructured SnTe. *Proc. Natl Acad. Sci. USA* **110**, 13261–13266 (2013).
10. Klemens, P. G. The scattering of low-frequency lattice waves by static imperfections. *Proc. Phys. Soc. A* **68**, 1113–1128 (1955).
11. Carruthers, P. Scattering of phonons by elastic strain fields and the thermal resistance of dislocations. *Phys. Rev.* **114**, 995–1001 (1959).
12. Kogure, Y. & Hiki, Y. Scattering of lattice waves by static strain fields in crystals. *J. Phys. Soc. Jpn* **36**, 1597–1607 (1974).
13. Kneeze, G. A. & Granato, A. V. Effect of independent and coupled vibrations of dislocations on low-temperature thermal conductivity in alkali halides. *Phys. Rev. B* **25**, 2851–2866 (1982).
14. Li, M. et al. Nonperturbative quantum nature of the dislocation–phonon interaction. *Nano Lett.* **17**, 1587–1594 (2017).
15. O'Hara, S. G. & Anderson, A. C. Scattering of thermal phonons by dislocations in superconducting lead and tantalum. *Phys. Rev. B* **10**, 574–579 (1974).
16. Nihira, T. & Iwata, T. Thermal resistivity changes in electron-irradiated pyrolytic-graphite. *Jpn J. Appl. Phys.* **14**, 1099–1104 (1975).
17. Jo, I., Pettes, M. T., Ou, E., Wu, W. & Shi, L. Basal-plane thermal conductivity of few-layer molybdenum disulfide. *Appl. Phys. Lett.* **104**, 201902 (2014).
18. Sun, B. et al. Temperature dependence of anisotropic thermal conductivity tensor of bulk black phosphorus. *Adv. Mater.* **29**, 1603297 (2017).
19. Sproull, R. L., Moss, M. & Weinstock, H. Effect of dislocations on the thermal conductivity of lithium fluoride. *J. Appl. Phys.* **30**, 334–337 (1959).
20. Su, Z. et al. Layer-by-layer thermal conductivities of the Group III nitride films in blue/green light emitting diodes. *Appl. Phys. Lett.* **100**, 201106 (2012).
21. Mion, C., Muth, J. F., Preble, E. A. & Hanser, D. Accurate dependence of gallium nitride thermal conductivity on dislocation density. *Appl. Phys. Lett.* **89**, 092123 (2006).
22. Loitsch, B., Schuster, F., Stutzmann, M. & Koblmüller, G. Reduced threading dislocation densities in high-*T*/N-rich grown InN films by plasma-assisted molecular beam epitaxy. *Appl. Phys. Lett.* **102**, 051916 (2013).
23. Ju, J. et al. Trade-off between morphology, extended defects, and compositional fluctuation induced carrier localization in high In-content InGaN films. *J. Appl. Phys.* **116**, 053501 (2014).
24. Gallinat, C. S., Koblmüller, G., Wu, F. & Speck, J. S. Evaluation of threading dislocation densities in In- and N-face InN. *J. Appl. Phys.* **107**, 053517 (2010).
25. Cahill, D. G. Analysis of heat flow in layered structures for time-domain thermoreflectance. *Rev. Sci. Instrum.* **75**, 5119–5122 (2004).
26. Sun, B. & Koh, Y. K. Understanding and eliminating artifact signals from diffusely scattered pump beam in measurements of rough samples by time-domain thermoreflectance (TDTR). *Rev. Sci. Instrum.* **87**, 064901 (2016).
27. Feser, J. P., Liu, J. & Cahill, D. G. Pump–probe measurements of the thermal conductivity tensor for materials lacking in-plane symmetry. *Rev. Sci. Instrum.* **85**, 104903 (2014).
28. Jiang, P., Huang, B. & Koh, Y. K. Accurate measurements of cross-plane thermal conductivity of thin films by dual-frequency time-domain thermoreflectance (TDTR). *Rev. Sci. Instrum.* **87**, 075101 (2016).
29. Luckyanova, M. N. et al. Anisotropy of the thermal conductivity in GaAs/AlAs superlattices. *Nano Lett.* **13**, 3973–3977 (2013).
30. Kwon, S., Zheng, J., Wingert, M. C., Cui, S. & Chen, R. Unusually high and anisotropic thermal conductivity in amorphous silicon nanostructures. *ACS Nano* **11**, 2470–2476 (2017).
31. Jiang, P., Lindsay, L., Huang, X. & Koh, Y. K. Interfacial phonon scattering and transmission loss in >1 μm thick silicon-on-insulator thin films. *Phys. Rev. B* **97**, 195308 (2018).
32. Jiang, P., Lindsay, L. & Koh, Y. K. Role of low-energy phonons with mean-free-paths >0.8 μm in heat conduction in silicon. *J. Appl. Phys.* **119**, 245705 (2016).
33. Vermeersch, B., Carrete, J. & Mingo, N. Cross-plane heat conduction in thin films with ab-initio phonon dispersions and scattering rates. *Appl. Phys. Lett.* **108**, 193104 (2016).
34. Dong, Z. S. & Zhao, C. W. Measurement of strain fields in an edge dislocation. *Physica B Condens. Matter* **405**, 171–174 (2010).
35. Katcho, N. A., Carrete, J., Li, W. & Mingo, N. Effect of nitrogen and vacancy defects on the thermal conductivity of diamond: an ab initio Green's function approach. *Phys. Rev. B* **90**, 094117 (2014).

Acknowledgements

The authors thank R. Wang and B. Huang at NUS for help with the thermal evaporation of Al films. The authors thank M. Li at MIT for explanation of his papers. This work was supported by an NUS Start-up Grant, the Singapore Ministry of Education Academic Research Fund Tier 2 under award no. MOE2013-T2–2–147 and Singapore Ministry of Education Academic Research Fund Tier 1 FRC project FY2016. C.P. and L.L. acknowledge support from the US Department of Energy, Office of Science, Basic Energy Sciences, Materials Sciences and Engineering Division and computational resources from the National Energy Research Scientific Computing Center (NERSC), a DOE Office of Science User Facility supported by the Office of Science of the US Department of Energy under contract no. DE-AC02-05CH11231. G.K. acknowledges support from the excellence program Nanosystems Initiative Munich (NIM) funded by the German Research Foundation (DFG).

Author contributions

G.K. and Y.K.K. initialized the idea. B.S. and Y.K.K. designed the experiments. B.S. performed the TDTR measurements and analysed the data. G.H., J.Z.J. and G.K. prepared and characterized the InN samples. C.P. and L.L. performed the first-principles and phonon-defect scattering calculations. All authors discussed the results and contributed to the manuscript.

Competing interests

The authors declare no competing interests.

Additional information

Supplementary information is available for this paper at https://doi.org/10.1038/s41563-018-0250-y.

Reprints and permissions information is available at www.nature.com/reprints.

Correspondence and requests for materials should be addressed to Y.K.K.

Publisher's note: Springer Nature remains neutral with regard to jurisdictional claims in published maps and institutional affiliations.

Methods

InN film synthesis with highly oriented threading dislocations. PAMBE was used to grow In-polar InN thin films on *c*-plane, (0001)-oriented GaN/sapphire substrates with an $In_{0.8}Ga_{0.2}N$ buffer layer. PAMBE growth of InN films on *c*-plane GaN is well known to produce single-crystalline films[36,37], but with a high density of threading dislocation defects due to the large lattice mismatch[27–29]. Both the InGaN buffer layer and subsequent InN film were grown under metal-rich (that is, In-rich) growth conditions to produce single-crystalline films with smooth surface morphology and high-quality, electronic-grade properties[22,23,36,38]. Due to the metal-rich conditions, macroscopic In droplets typically accumulate at the growth surface[37]; these were subsequently removed in buffered hydrochloric (HCl) acid to produce specular, atomically smooth surfaces for TDTR measurements.

In our sample structure, we implemented an $In_xGa_{1-x}N$ buffer layer ($x=0.8$) (Fig. 1a), which serves two purposes. First, the low thermal conductivity of this buffer layer forces heat to flow in the in-plane direction within the InN films. As a result, heat dissipation in our measurements is sensitive to the in-plane thermal conductivity of InN even at 80 K, and in-plane thermal conductivities can be measured accurately (see Fig. 1b for illustration). Second, the high-In-content $In_{0.8}Ga_{0.2}N$ buffer layer is implemented to reduce the lattice mismatch between the epitaxial InN film and the GaN substrate, such that the largest portion of mismatch strain is relieved within the buffer layer. Thereby, non-vertically oriented threading dislocations, which also form during heteroepitaxial nucleation of group-III nitride films near the substrate interface[22,39], are readily annihilated within the $In_{0.8}Ga_{0.2}N$ buffer layer—a process that is driven by the merging of two inclined threading dislocations with opposite Burgers vector[39]. As a result, the largest fraction of threading dislocations propagating in the InN film are relatively well-oriented along the vertical *c* axis (that is, (0001) orientation), which we refer to as the cross-plane direction. As shown in Fig. 1c–f, inclined dislocations are also formed; however, they are predominantly located in the $In_{0.8}Ga_{0.2}N$ buffer layer, where they fuse and annihilate[39].

To realize variation in the dominant edge-type threading dislocation density we varied the growth temperature for the InN films between 450 °C and 500 °C, in accordance with ref. [36]. Hereby, higher growth temperature yields a lower dislocation density compared to low growth temperatures. In total, we explored four samples with different threading dislocation densities in the InN films, ranging from $1.1\times10^{10}\,cm^{-2}$ to $2.9\times10^{10}\,cm^{-2}$.

TDTR. The TDTR measurements were carried out as reported in refs [18,26,40], and are reproduced here for completeness. We coated a thin Al layer (~100 nm) on the samples for TDTR measurements. Laser pulses from an ultrafast laser were split into a pump and a probe beam. The pump beam heated the samples periodically, creating a temperature oscillation. The probe beam monitored the temperature oscillation at the sample surfaces through thermoreflectance (that is, change of reflectance with temperature). Because the induced temperature oscillation depends on the thermal properties of each sample, the thermal conductivity can be extracted. The thermal conductivity of the samples is derived by comparing the measured cooling curves to calculations of a thermal model[25]. In this study, we used a $1/e^2$ laser radius of 5 μm and a modulation frequency of 0.5 MHz for in-plane thermal measurements, and 28 μm and 10 MHz for cross-plane thermal measurements. To measure the cross-plane thermal conductivity at 80, 100 and 120 K we used a modulation frequency of 22.2 MHz for improved sensitivity. To improve the accuracy, we also independently measured the thermal conductivity of the buffer InGaN layer (Supplementary Note 2.3). The uncertainties in our measurements of in-plane and cross-plane thermal conductivity are estimated as 12 and 10% at room temperature, and 13 and 40% at 80 K. Details are provided in Supplementary Note 2.5.

Reduction of the apparent thermal conductivity in TDTR measurements arising from non-Fourier heat transport, such as frequency[41] and spot-size dependences[42], can affect the determination of intrinsic thermal conductivity. These effects were extensively explored for measurements of phonon mean free paths[41–43], and can originate from, for example, ballistic phonon transport[41,44] or superdiffusive Lévy transport[45]. In this study, we did not observe spot size and frequency dependences in the TDTR measurements of the InN films (see Supplementary Note 2.4 and Supplementary Fig. 8 for TDTR data at different spot sizes and modulation frequencies). The lack of spot size and frequency dependences in our measurements is consistent with the previous discovery that non-equilibrium effects are less pronounced in thin films[31], because additional boundary scattering reduces the distribution of phonon mean free paths in thin films.

Density functional theory calculations. The thermal conductivity of in-plane and cross-plane InN was calculated by self-consistently solving the Peierls–Boltzmann transport (PBT) equation[46–48]. Three-phonon and phonon–isotope scattering rates were considered within first-order perturbation theory as described in previous numerical works[3,49–53]. These rates were combined with empirical phonon–dislocation scattering rates derived by Klemens[10] and Carruthers[11] using Matheissen's rule, and the PBT equation then solved. Further details of the implementation of this methodology and description of the empirical phonon–dislocation scattering rates are provided in Supplementary Note 4.

Data availability

The data sets generated during and/or analysed during the current study are available from the corresponding author on reasonable request.

References

36. Masataka, H. & Toshiaki, M. High-quality InN film grown on a low-temperature-grown GaN intermediate layer by plasma-assisted molecular-beam epitaxy. *Jpn J. Appl. Phys.* **41**, L540 (2002).
37. Yoshiki, S., Nobuaki, T., Akira, S., Tsutomu, A. & Yasushi, N. Growth of high-electron-mobility InN by RF molecular beam epitaxy. *Jpn J. Appl. Phys.* **40**, L91 (2001).
38. Gallinat, C. S. et al. In-polar InN grown by plasma-assisted molecular beam epitaxy. *Appl. Phys. Lett.* **89**, 032109 (2006).
39. Romanov, A. E. & Speck, J. S. Stress relaxation in mismatched layers due to threading dislocation inclination. *Appl. Phys. Lett.* **83**, 2569–2571 (2003).
40. Huang, B. & Koh, Y. K. Improved topological conformity enhances heat conduction across metal contacts on transferred graphene. *Carbon* **105**, 268–274 (2016).
41. Koh, Y. K. & Cahill, D. G. Frequency dependence of the thermal conductivity of semiconductor alloys. *Phys. Rev. B* **76**, 075207 (2007).
42. Minnich, A. J. et al. Thermal conductivity spectroscopy technique to measure phonon mean free paths. *Phys. Rev. Lett.* **107**, 095901 (2011).
43. Regner, K. T. et al. Broadband phonon mean free path contributions to thermal conductivity measured using frequency domain thermoreflectance. *Nat. Commun.* **4**, 1640 (2013).
44. Wilson, R. B. & Cahill, D. G. Anisotropic failure of Fourier theory in time-domain thermoreflectance experiments. *Nat. Commun.* **5**, 5075 (2014).
45. Mohammed, A. M. S. et al. Fractal Lévy heat transport in nanoparticle embedded semiconductor alloys. *Nano Lett.* **15**, 4269–4273 (2015).
46. Peierls, R. E. *Quantum Theory of Solids* (Clarendon Press, 1955).
47. Ziman, J. M. *Electrons and Phonons. The Theory of Transport Phenomena in Solids* (Oxford Univ. Press, Oxford, 1960).
48. Srivastava, G. P. *The Physics of Phonons* (Taylor & Francis, Abingdon, 1990).
49. Omini, M. & Sparavigna, A. Beyond the isotropic-model approximation in the theory of thermal conductivity. *Phys. Rev. B* **53**, 9064–9073 (1996).
50. Lindsay, L., Broido, D. A. & Reinecke, T. L. Thermal conductivity and large isotope effect in GaN from first principles. *Phys. Rev. Lett.* **109**, 095901 (2012).
51. Lindsay, L., Broido, D. A. & Reinecke, T. L. Ab initio thermal transport in compound semiconductors. *Phys. Rev. B* **87**, 165201 (2013).
52. Mingo, N., Stewart, D. A., Broido, D. A., Lindsay, L. & Li, W. in *Length-Scale Dependent Phonon Interactions* (eds Shindé, S. L. & Srivastava, G. P.) 137–173 (Springer, New York, 2014).
53. Lindsay, L. First principles Peierls–Boltzmann phonon thermal transport: a topical review. *Nanosc. Microsc. Therm.* **20**, 67–84 (2016).